Modeling the Atmospheric Phase Effects of a Digital Antenna Array Communications System

A. Tkacenko[1]

In an antenna array system such as that used in the Deep Space Network (DSN) for satellite communication, it is often necessary to account for the effects due to the atmosphere. Typically, the atmosphere induces amplitude and phase fluctuations on the transmitted downlink signal that invalidate the assumed stationarity of the signal model. The degree to which these perturbations affect the stationarity of the model depends both on parameters of the atmosphere, including wind speed and turbulence strength, and on parameters of the communication system, such as the sampling rate used. In this article, we focus on modeling the atmospheric phase fluctuations in a digital antenna array communications system. Based on a continuous-time statistical model for the atmospheric phase effects, we show how to obtain a related discrete-time model based on sampling the continuous-time process. The effects of the nonstationarity of the resulting signal model are investigated using the sample matrix inversion (SMI) algorithm for minimum mean-squared error (MMSE) equalization of the received signal.

I. Introduction

In a typical antenna array-based digital communications system, such as that used in the Deep Space Network (DSN), it is often necessary to account for effects due to the atmosphere. The atmosphere, which comprises the medium between the transmit antenna (typically a satellite in orbit) and the receive antennas (typically an array of terrestrial-based antennas), induces amplitude and phase fluctuations on the transmitted downlink signal [1]. These fluctuations or perturbations are often time-varying in nature, invalidating the stationarity of the signal model that is commonly assumed.

If these fluctuations vary slowly enough, then commonly used adaptive algorithms for combining the received signals, such as the sample matrix inversion (SMI) or least mean-squares (LMS) algorithms [2], can be used to track the variations. On the other hand, if the atmospheric effects vary too quickly, then it is often difficult, if not impossible, to track the fluctuations and recover the transmitted signal. The degree of nonstationarity due to the effects of the atmosphere largely depends on properties of the atmosphere itself, including wind speed and turbulence strength, as well as properties of the digital communications system employed, such as the sampling rate used at the receiver.

In this article, we analyze the effects of atmospheric phase variations on a digital antenna array communications signal. The continuous-time atmospheric phase processes are modeled by a wide sense stationary (WSS) statistical characterization originally introduced by Treuhaft and Lanyi [3]. From this continuous-time model, we derive a related discrete-time model for the atmospheric phase processes based on a sampled version of the phase processes. The degree of nonstationarity imparted by the atmospheric phase effects is analyzed experimentally through simulations using the SMI algorithm for combining of the array outputs.

A. Outline

In Section II, we review the baseband model for the antenna array digital communications signal. There, we show step by step the complete communication path link from the transmitter to the channel to the receiver. In Section III, we review the continuous-time WSS model for the atmospheric phase processes as derived by Treuhaft and Lanyi [3]. From this model, we show in Section IV how to obtain a related discrete-time WSS characterization for the sampled continuous-time atmospheric phase processes. In Section V, simulation results for acquisition in the presence of atmospheric phase effects are presented using the SMI algorithm. There, the effects due to the nonstationarity imparted by the atmosphere are shown. Finally, concluding remarks are made in Section VI.

B. Notations

All notations are as in [4] unless stated otherwise. In particular, continuous-time frequencies will be denoted by uppercase letters (i.e., Ω for radian and F for normalized frequencies), whereas discrete-time frequencies will be denoted by lowercase letters (i.e., ω and f). Furthermore, boldfaced lowercase letters (such as $\mathbf{v}$) will be used to denote vectors, while boldfaced uppercase letters (such as $\mathbf{A}$) will be used to denote matrices. One notable exception to the notation used in [4] is that continuous-time signal variables will be enclosed by parentheses, whereas discrete-time signal variables will be enclosed by brackets. For example, the notation $x(t)$ refers to a continuous-time function of the variable $t \in \mathbb{R}$, whereas $x[n]$ refers to a discrete-time function of the variable $n \in \mathbb{Z}$.

II. Antenna Array Digital Communications Baseband Signal Model

Prior to introducing a statistical description of the atmospheric phase processes, it is worthwhile to review a fundamental model of the communications system used by the antenna array. In this section, we present a baseband model for the digital communications system employed by the antenna array. We will cover a simplified model, starting from the transmitter, progressing to the channel paths, and finally ending at the receiver.

Although the goal between the transmitter and receiver is the transmission of a digital signal, the medium separating the two is an analog one, which requires that the digital signal be converted to an analog signal (such as a voltage waveform) prior to being sent through the medium. Furthermore, the receiver must be able to recover the desired digital signal from the received analog signals. A pictorial description of this scenario in the analog domain is shown in Fig. 1.

In this setting, we have 1 transmit antenna (for example, a satellite in orbit) trying to communicate with N receive antennas (such as an array of terrestrial antennas). Such a system is known as a single input–multiple output (SIMO) system [4]. Along each path from the transmitter to the receiver, the transmitted signal incurs delays and distortions due to the position of the receive antennas as well as effects from the atmosphere [1,5]. In addition, the transmitted signal could be corrupted by noise as well as other interferers [5]. Prior to analyzing the effects of the analog channel, we will first review how to generate the transmitted analog baseband signal $s(t)$ from a set of input digital data.

A. Transmitted Signal Model

A baseband model for generating the transmitted analog signal $s(t)$ from Fig. 1 is shown in Fig. 2. Here, the discrete-time digital information source $d[n]$ consists of complex data symbols d_n. These symbols are typically from a special data constellation such as an M-ary phase shift keying (M-PSK) or a quadrature amplitude modulation (QAM) constellation [6].

The discrete-time signal $d[n]$ is converted to an analog signal using a digital-to-analog (D/A) converter. Here, the D/A converter generates an impulse train of *Dirac delta functions* [4] separated in time by an amount T_b, which we call the *baud interval* or *symbol interval* [6]. An equivalent measure of this time is the *baud rate* or *symbol rate* defined by $\mathcal{R}_b \triangleq 1/T_b$. The impulse train $d(t)$ is then filtered by a *pulse-shaping filter* $p(t)$ [6] and scaled by a positive gain factor of A to produce the output baseband transmitted signal $s(t)$.[2]

Although the pulse-shaping filter $p(t)$ can be any arbitrary shape, to prevent intersymbol interference (ISI) [6], the pulse typically is chosen to satisfy the *Nyquist* (T_b) *criterion* [4], given below as follows:
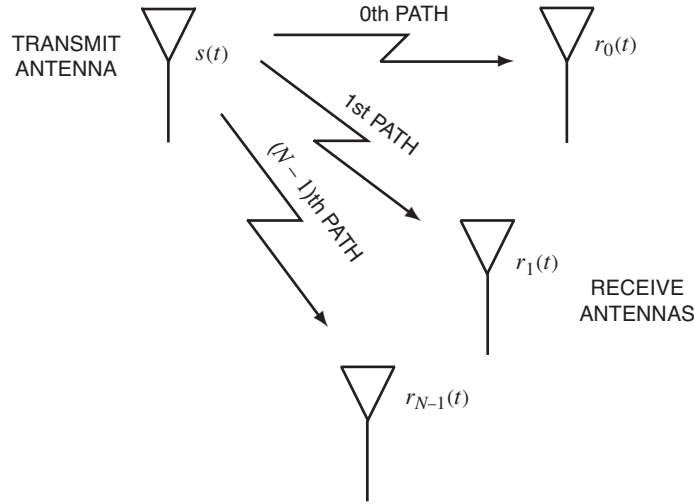

Fig. 1. Pictorial description of the analog link between the transmitter and receiver in an antenna array system.
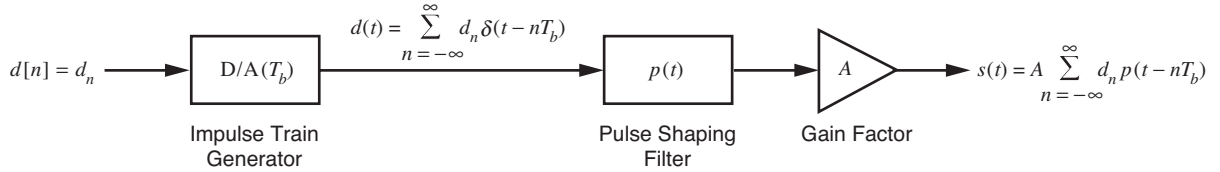

Fig. 2. Baseband transmitter signal model.

---

[2] In a realistic implementation of the transmitter system, the impulse train generator and pulse-shaping filter operations are combined into one operation to generate the transmitted signal $s(t)$ from the information source $d[n]$. We have opted to keep these operations separate here in order to make the receiver system appear more mathematically complementary to the transmitter system, as can be seen later on in Section II.C.

$$\frac{1}{T_b} \int_{-\infty}^{\infty} p(t)p^* \left(t - nT_b\right) \, dt = \delta_n \tag{1}$$

where δ_n is the *Kronecker delta function* [4] given by

$$\delta_n = \begin{cases} 1, & n = 0 \\ 0, & n \neq 0, n \in \mathbb{Z} \end{cases}$$

Examples of Nyquist (T_b) pulse shapes include time-limited pulses such as the non-return-to-zero (NRZ) pulse [6],

$$p_{\mathrm{NRZ}}(t) = \begin{cases} 1, & 0 \leq t < T_b \\ 0, & \text{otherwise} \end{cases} \tag{2}$$

as well as band-limited pulses such as the sinc pulse [6],

$$p_{\mathrm{sinc}}(t) = \mathrm{sinc} \left(\frac{t}{T_b}\right)$$

where $\mathrm{sinc}\,(x) \triangleq [\sin\,(\pi x)\,/\pi x]$. Expressions for other common pulse shapes used, such as the Manchester, raised cosine, and Gaussian minimum shift keying (GMSK)-type pulses, can be found in [5,6].

B. Continuous-Time Channel Path Model

Once the discrete-time information source $d[n]$ has been converted to a continuous-time signal $s(t)$, it is broadcast over the transmitter to the receiver antennas as shown in Fig. 1. Although there are many ways in which to model the effects of the channel, the most common way to do so is to model the channel as a linear time-varying distortion with additive noise [5]. This is shown in Fig. 3 for the kth channel path for $0 \leq k \leq N - 1$.

Here $u_k(t)$, the output of the linear time-varying system, is given by

$$u_k(t) = \int_{-\infty}^{\infty} h_k(\tau, t)s\left(t - \tau\right) d\tau \tag{3}$$

where $h_k(\tau, t)$ is the *impulse response* of the linear time-varying system [5] [i.e., $h_k(t - \tau, t)$ is the output of the system in response to the input $\delta(t - \tau)$]. For a terrestrial wireless setting, the impulse response
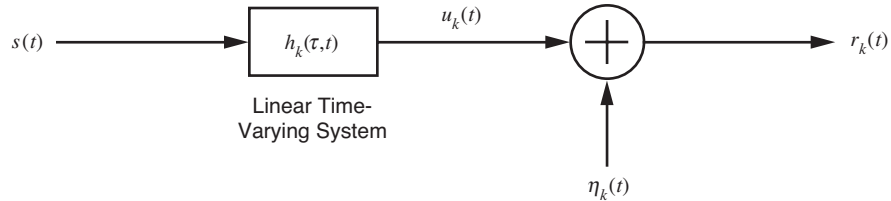

Fig. 3. Baseband analog channel model of the kth transmission path from Fig 1.

$h_k(\tau, t)$ typically consists of several multipath components along with a possible *specular* or *line-of-sight* (LOS) component [5]. In contrast to this, for an antenna array system such as that used in the DSN, the presence of multipath components will appear as very weak and the only dominant part will be the specular component [1]. For an array of this type, the impulse response $h_k(\tau, t)$ is given by

$$h_k(\tau, t) = \alpha_k(t)\delta\big(\tau - \tau_k(t)\big) \qquad (4)$$

where $\alpha_k(t)$ is a complex time-varying scale factor and $\tau_k(t)$ is a time-varying delay parameter.

For the DSN application under consider, the scale $\alpha_k(t)$ accounts for both the receiver array geometry as well as atmospheric effects. Here, we model this scale factor as follows [1]:

$$\alpha_k(t) = \rho_{k;g} e^{j(\phi_{k;g} + \theta_{k;a}(t))} \qquad (5)$$

where $\rho_{k;g}$ and $\phi_{k;g}$ are, respectively, the gain and phase incurred as a result of the receiver array *geometry* (both of which are assumed to be constant with time), and $\theta_{k;a}(t)$ denotes the phase perturbation caused by the *atmosphere* (which does vary with time).

The delay parameter $\tau_k(t)$ typically is modeled as follows for an array system such as that used by the DSN:

$$\tau_k(t) = \tau_{k;g} \qquad (6)$$

where $\tau_{k;g}$ is a constant delay incurred as a result of the receiver array geometry. For example, for a uniform linear array, the delay is given by [1]

$$\tau_{k;g} = \tau_0 + \frac{kd}{c}\sin\psi, \ 0 \le k \le N-1$$

where τ_0 is a constant delay offset, d is the spacing between the array elements, c is the speed of the transmitted waveform in the atmospheric medium (most often the speed of light), and ψ is the azimuthal angle of the transmit antenna with respect to the receive antennas [1].

The additive noise component $\eta_k(t)$ is modeled as a circular complex additive white Gaussian noise (AWGN) process with mean 0 and power spectral density (psd) N_0 [5]. This is equivalent to saying that the real and imaginary parts of $\eta_k(t)$ are uncorrelated real Gaussian processes with mean 0 and psd $N_0/2$. Mathematically, this implies that we have the following:

$$E\big[\eta_k(t)\big] = 0 \qquad (7)$$

$$E\big[\eta_k(t)\eta_k(t-\tau)\big] = 0 \qquad (8)$$

$$E\big[\eta_k(t)\eta_k^*(t-\tau)\big] = N_0\delta(\tau) \qquad (9)$$

Furthermore, the real and imaginary parts of the processes $\eta_k(t)$ and $\eta_\ell(t)$ are assumed to be uncorrelated for all $k \ne \ell$. This implies the following:

$$E\big[\eta_k\left(t_0\right)\eta_\ell\left(t_1\right)\big] = E\big[\eta_k\left(t_0\right)\eta_\ell^*\left(t_1\right)\big] = 0\,, \forall\, t_0, t_1, k \neq \ell \tag{10}$$

C. Received Signal Model

Upon obtaining the analog outputs of the array channel at the receiver antennas, these continuous-time signals must be converted back to a discrete-time format. This typically is done using the system shown in Fig. 4. Note that this system is symmetric or complementary with respect to the transmitter system of Fig. 2. First, the received analog signal is filtered by the *matched filter* [6] for the original pulse shape $p(t)$, which is simply $p^*\left(-t\right)$.[3] The impetus for using the matched filter comes from *maximum likelihood* (ML) estimation theory [6] for estimation of the information source $d[n]$ in the presence of AWGN. (It should be noted that oftentimes in an antenna-array-type environment, prior to the matched filtering operation, the incoming analog signal $r_k(t)$ is *delay compensated* [1] to account for the delays incurred by the channel. This compensation incorporates knowledge from predicts to estimate the path delays $\tau_k(t)$ from Eq. (6). Equivalently, this can be achieved mathematically by setting the path delays to zero (i.e., $\tau_k(t) = 0$ for all k and t).)
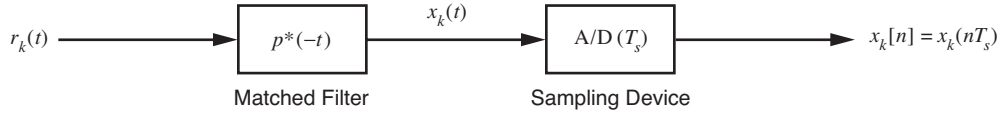

Fig. 4. Baseband receiver signal model.

After matched filtering, the resulting signal $x_k(t)$ is converted to a digital signal through an analog-to-digital (A/D) converter [4] that simply samples $x_k(t)$ at $t = nT_s$. Here, T_s is known as the *sampling interval* [4]. Equivalently, this interval can be described by the *sampling frequency* or *sampling rate* defined to be $F_s \triangleq 1/T_s$. In order to recover the original information source $d[n]$, the sampling rate F_s must be at least equal to the baud rate $\mathcal{R}_b$ (i.e., we need $F_s \geq \mathcal{R}_b$) [5,6]. By oversampling the output (i.e., when we have $F_s > \mathcal{R}_b$), we receive additional information about the underlying transmitted signal that can be used to achieve a form of *temporal diversity* [5]. This is in addition to the inherent *spatial receive diversity* [5] that we have due to the fact that we are using multiple receive antennas.

Assuming that the delays from the channel have been compensated and that the sampling rate F_s equals the baud rate $\mathcal{R}_b$, then from Eqs. (5), (4), and (3), and Figs. 4, 3, and 2, we have the following:

$$x_k[n] = x_k\left(nT_s\right) = \int_{-\infty}^{\infty} r_k(\tau)p^*\left(\tau - nT_s\right)\,d\tau$$

$$= \int_{-\infty}^{\infty} u_k(\tau)p^*\left(\tau - nT_s\right)\,d\tau + \underbrace{\int_{-\infty}^{\infty} \eta_k(\tau)p^*\left(\tau - nT_s\right)\,d\tau}_{v_k[n]} \tag{11}$$

$$= \int_{-\infty}^{\infty} \alpha_k(\tau)s\big(\tau - \tau_k(\tau)\big)p^*\left(\tau - nT_s\right)\,d\tau + v_k[n]$$

$$= \rho_{k;g}e^{j\phi_{k;g}}\int_{-\infty}^{\infty} e^{j\theta_{k;a}(\tau)}s(\tau)p^*\left(\tau - nT_s\right)\,d\tau + v_k[n] \tag{12}$$

---

[3] In many digital communications textbooks, the pulse shape $p(t)$ is time-limited to some interval $t \in [0, T)$, and the corresponding matched filter is implemented as $p^*\left(T - t\right)$ in order to make it causal [4]. We omit this delay here as it simplifies the underlying mathematics.

Here, Eq. (12) follows from the fact that we have assumed that the delays from the channel have been compensated.

Before proceeding further with the analysis of $x_k[n]$, let us first consider the filtered discrete-time noise process $v_k[n]$ defined in Eq. (11). Note that we have the following:

$$E\big[v_k[n]\big] = \int_{-\infty}^{\infty} E\big[\eta_k(n)\big] p^*(\tau - nT_s)\, d\tau = 0 \tag{13}$$

$$E\big[v_k[n]v_k[n-m]\big] = \int_{-\infty}^{\infty}\int_{-\infty}^{\infty} E\big[\eta_k(\tau_0)\eta_k(\tau_1)\big] p^*(\tau_0 - nT_s)p^*\big(\tau_1 - (n-m)T_s\big)\, d\tau_0\, d\tau_1$$

$$= 0 \tag{14}$$

$$E\big[v_k[n]v_k^*[n-m]\big] = \int_{-\infty}^{\infty}\int_{-\infty}^{\infty} E\big[\eta_k(\tau_0)\eta_k^*(\tau_1)\big] p^*(\tau_0 - nT_s)p\big(\tau_1 - (n-m)T_s\big)\, d\tau_0\, d\tau_1$$

$$= \int_{-\infty}^{\infty}\int_{-\infty}^{\infty} N_0\delta\,(\tau_0 - \tau_1)\, p^*(\tau_0 - nT_b)p\big(\tau_1 - (n-m)T_b\big)\, d\tau_0\, d\tau_1 \tag{15}$$

$$= N_0 \int_{-\infty}^{\infty} p^*(\tau - nT_b)p\big(\tau - (n-m)T_b\big)\, d\tau$$

$$= N_0 \int_{-\infty}^{\infty} p(\lambda)p^*(\lambda - mT_b)\, d\lambda$$

$$= N_0 T_b \delta_m \tag{16}$$

Here, Eq. (13) follows from Eq. (7); Eq. (14) follows from Eq. (8); and Eq. (15) follows from Eq. (9) and the fact that $T_s = T_b$ here. For Eq. (16), we used the fact that the pulse shape was assumed to satisfy the Nyquist (T_b) criterion of Eq. (1). Given that the continuous-time process $\eta_k(t)$ is Gaussian, it follows that the discrete-time process $v_k[n]$ is also Gaussian. From Eqs. (13), (14), and (16), we conclude that $v_k[n]$ is a discrete-time AWGN process. As $\eta_k(t)$ and $\eta_\ell(t)$ satisfy Eq. (10), it can be shown that we have

$$E\big[v_k\,[n_0]\,v_\ell\,[n_1]\,\big] = E\big[v_k\,[n_0]\,v_\ell^*\,[n_1]\,\big] = 0\,,\ \forall\, n_0, n_1, k \neq \ell \tag{17}$$

and hence the discrete-time processes $v_k[n]$ and $v_\ell[n]$ are uncorrelated.

To proceed with the analysis of $x_k[n]$, from here on in, we will assume that the pulse shape used is the NRZ pulse of Eq. (2). In this case, we have, from Eq. (12),

$$x_k[n] = \rho_{k;g}e^{j\phi_{k;g}} \int_{nT_s}^{(n+1)T_s} e^{j\theta_{k;a}(\tau)} s(\tau)\, d\tau + v_k[n] \tag{18}$$

At this point, we will assume that the sampling rate F_s is much larger than the rate of change of the atmospheric phase process. In other words, we will assume that T_s is small enough that the function

$\theta_{k;a}(t)$ is approximately constant over the interval $t \in \left[nT_s, (n+1)T_s\right)$. Here, we will assume that we have

$$\theta_{k;a}(t) \approx \theta_{k;a}(nT_s), \ \forall \ t \in \left[nT_s, (n+1)T_s\right) \tag{19}$$

In Section III, we will justify this approximation. Using Eq. (19) in Eq. (18), we get the following:

$$x_k[n] = \rho_{k;g} e^{j\phi_{k;g}} e^{j\theta_{k;a}(nT_s)} \int_{nT_s}^{(n+1)T_s} s(\tau) \, d\tau + v_k[n]$$

$$= \rho_{k;g} e^{j\phi_{k;g}} e^{j\theta_{k;a}(nT_s)} A \sum_{m=-\infty}^{\infty} d_m \int_{nT_s}^{(n+1)T_s} p_{\mathrm{NRZ}}\left(\tau - mT_s\right) \, d\tau + v_k[n]$$

$$= A\rho_{k;g} e^{j\phi_{k;g}} e^{j\theta_{k;a}(nT_s)} \sum_{m=-\infty}^{\infty} d_m T_b \delta_{m-n} + v_k[n]$$

$$= AT_b \rho_{k;g} e^{j\phi_{k;g}} e^{j\theta_{k;a}(nT_s)} d_n + v_k[n] \tag{20}$$

Defining the discrete-time process $\beta_k[n]$ as follows,

$$\beta_k[n] \triangleq \theta_{k;a}(nT_s) \tag{21}$$

and using the fact that the information source $d[n]$ is given by $d[n] = d_n$, from Eq. (20), we have

$$x_k[n] = e^{j\beta_k[n]} AT_b \rho_{k;g} e^{j\phi_{k;g}} d[n] + v_k[n] \tag{22}$$

1. Vector/Matrix Representation of the Received Array Signals. Let us define the following vectors and matrices:[4]

$$\mathbf{x}[n] \triangleq \begin{bmatrix} x_0[n] \\ x_1[n] \\ \vdots \\ x_{N-1}[n] \end{bmatrix}, \ \mathbf{B}[n] \triangleq \mathrm{diag}\left(e^{j\beta_0[n]}, e^{j\beta_1[n]}, \cdots, e^{j\beta_{N-1}[n]}\right) \tag{23}$$

$$\mathbf{a} \triangleq \begin{bmatrix} AT_b\rho_{0;g} e^{j\phi_{0;g}} \\ AT_b\rho_{1;g} e^{j\phi_{1;g}} \\ \vdots \\ AT_b\rho_{N-1;g} e^{j\phi_{N-1;g}} \end{bmatrix}, \ \mathbf{v}[n] \triangleq \begin{bmatrix} v_0[n] \\ v_1[n] \\ \vdots \\ v_{N-1}[n] \end{bmatrix} \tag{24}$$

Here $\mathbf{x}[n]$, $\mathbf{a}$, and $\mathbf{v}[n]$ are all $N \times 1$ column vectors whereas $\mathbf{B}[n]$ is an $N \times N$ matrix. From the definitions given in Eqs. (23) and (24), it can be seen that from Eq. (22) we have the following vector/matrix equation:

---

[4] Here, the notation $\mathrm{diag}\left(x_0, x_1, \cdots, x_{N-1}\right)$ denotes an $N \times N$ diagonal matrix whose kth diagonal element is equal to x_k.

$$\mathbf{x}[n] = \mathbf{B}[n]\mathbf{a}d[n] + \mathbf{v}[n] \tag{25}$$

From Eq. (25), it can be seen that $\mathbf{x}[n]$ consists of a linear time-varying scaled version of the desired scalar information source $d[n]$ along with an additive vector noise process $\mathbf{v}[n]$. Combining Eq. (24) with Eqs. (13), (14), (16), and (17), it follows that $\mathbf{v}[n]$ is a discrete-time complex circular AWGN vector process [5] with mean $\mathbf{0}$ and covariance $\sigma^2\mathbf{I}$, where we have defined σ^2 as $\sigma^2 \triangleq N_0 T_b$. We will express this using the notation from [5] as

$$\mathbf{v}[n] \sim \mathcal{CN}(\mathbf{0}, \sigma^2\mathbf{I})$$

Note that $\mathbf{x}[n]$ from Eq. (25) consists of a signal component $\mathbf{B}[n]\mathbf{a}d[n]$ as well as a noise component $\mathbf{v}[n]$. One valid measure of the signal strength to the noise strength is the *signal-to-noise ratio* (SNR) [5,6], which is defined as follows:

$$\text{SNR}_{\mathbf{x}[n]} \triangleq \frac{\text{energy of signal component of } \mathbf{x}[n]}{\text{energy of noise component of } \mathbf{x}[n]} = \frac{\text{Tr}\left\{E\left[\left(\mathbf{B}[n]\mathbf{a}d[n]\right)\left(\mathbf{B}[n]\mathbf{a}d[n]\right)^\dagger\right]\right\}}{\text{Tr}\left\{E\left[\mathbf{v}[n]\mathbf{v}^\dagger[n]\right]\right\}} \tag{26}$$

where $\text{Tr}\{\cdot\}$ denotes the *trace* operator [4] (i.e., the sum of the diagonal elements of the input matrix) and $\dagger$ denotes the *transpose conjugate* operator [4]. Assuming that $d[n]$ comes from a unit energy constellation (so that $E\left[|d[n]|^2\right] = 1$), then from Eq. (26), we have

$$\text{SNR}_{\mathbf{x}[n]} = \frac{\mathbf{a}^\dagger\mathbf{a}}{N\sigma^2} = \left(\frac{A^2 T_b}{N_0}\right) \cdot \frac{1}{N} \sum_{n=0}^{N-1} \rho_{k;g}^2 \tag{27}$$

The SNR as well as the *combining loss* (which will be defined later in Section V) will be used to measure the tracking performance of the SMI algorithm in the presence of atmospheric phase effects.

III. Statistical Model for the Continuous-Time Atmospheric Phase Processes

In the previous section, a detailed analysis of the complete communication link between the transmitter and receiver was given. During the course of this analysis, a set of time-varying atmospheric phase processes $\{\theta_{k;a}(t)\}$ was introduced. In this section, we review a statistical model for this set of processes as based on the Treuhaft and Lanyi model given in [3].

Define the following $N \times 1$ vector of atmospheric phase processes:

$$\boldsymbol{\theta}(t) \triangleq \begin{bmatrix} \theta_{0;a}(t) \\ \theta_{1;a}(t) \\ \vdots \\ \theta_{N-1;a}(t) \end{bmatrix} \tag{28}$$

Here, we model the vector process $\boldsymbol{\theta}(t)$ as a *wide sense stationary* (WSS) random process [4]. This means that the mean $E[\boldsymbol{\theta}(t)]$ and autocorrelation $E\left[\boldsymbol{\theta}(t)\boldsymbol{\theta}^\dagger(t-\tau)\right]$ are independent of t. As such, we can define the mean and autocorrelation as follows:

$$\boldsymbol{\mu_{\theta}} \triangleq E\big[\boldsymbol{\theta}(t)\big]$$

$$\mathbf{R_{\theta\theta}}(\tau) \triangleq E\left[\boldsymbol{\theta}(t)\boldsymbol{\theta}^{\dagger}(t-\tau)\right]$$

Note that even if the vector process $\boldsymbol{\theta}(t)$ is WSS, the received signal vector $\mathbf{x}[n]$ from Eq. (25) is not because it contains exponentiated versions of the components of $\boldsymbol{\theta}(t)$.

Since the atmospheric phase processes are considered to be perturbations of the received signal phases, it is generally accepted that the atmospheric phases are zero mean, and so $\boldsymbol{\mu_{\theta}} = \mathbf{0}$. As far as the second-order statistics, $\mathbf{R_{\theta\theta}}(\tau)$, are concerned, in much of the literature, spatial correlations are modeled independently from temporal ones [1,3]. Due to the fact that we must *jointly* account for both phenomena here, this presents us with the dilemma of how to carry out this joint modeling.

Before proceeding with this joint model to obtain $\mathbf{R_{\theta\theta}}(\tau)$, we review the spatial and temporal phase correlation models given in [1,3]. In particular, we will focus on the models given by Treuhaft and Lanyi [3].

A. Review of Spatial and Temporal Models of the Atmospheric Phase Processes

1. Spatial Correlation Model. The phase perturbations caused by the atmosphere are typically due in large part to water vapor fluctuations in the troposphere [1,3]. In these cases, the *spatial refractivity structure function* [1], which we define below, can be approximated using Kolmogorov turbulence theory [1]. A better approximation for the spatial structure function is the one proposed by Treuhaft and Lanyi [3], which we describe below.

The spatial refractivity structure function $D_{\chi}(r)$ measures the difference of the refractive index of two points that are a distance of r from each other. It is defined as follows [1]:

$$D_{\chi}(r) \triangleq E\left[|\chi(r_0 - r) - \chi(r_0)|^2\right] \tag{29}$$

where $\chi(r)$ denotes the deviation of the refractive index from unity (i.e., $\chi(r) = \eta(r) - 1$, where $\eta(r)$ is the index of refraction [3]). From Eq. (29), we have implicitly assumed that the structure function depends only on the distance between the two locations $(r_0 + r)$ and r_0, and not on the actual reference point r_0. This stationarity assumption holds approximately for large patches of turbulence [1].

In classical Kolmogorov turbulence theory, $D_{\chi}(r)$ is approximated as [1]

$$D_{\chi}(r) = C^2 r^{2/3}$$

where C is a parameter known as the *turbulence strength* [1] and is nominally 2.4×10^{-7} m$^{-1/3}$. Although the Kolmogorov model is appropriate for small distances, it diverges as $r \to \infty$. Physically, this does not make sense as the correlation between locations infinitely far away should go to zero.

A more appropriate model for $D_{\chi}(r)$ is the one used by Treuhaft and Lanyi [3]:

$$D_{\chi}(r) = \frac{C^2 r^{2/3}}{1 + \left(\dfrac{r}{L}\right)^{2/3}} \tag{30}$$

where L is a parameter known as the *outer scale* of the turbulence [1]. Treuhaft and Lanyi chose a fairly large value for the outer scale (3,000 km) to be consistent with Kolmogorov's model over a large range of baseline distances. More recent studies, however, conducted at the Very Large Array (VLA) in Socorro, New Mexico, by Carilli and Holdaway [7] indicate that a more practical value for the outer scale is 6 km.

It can be shown that the *spatial* phase structure function $D_{\theta;s}(r)$ [1], defined by

$$D_{\theta;s}(r) \triangleq E\left[\left| \theta_s\left(r_0 + r\right) - \theta_s\left(r_0\right)\right|^2 \right] \tag{31}$$

which measures the deviation of the phase of the atmosphere at two points separated by a distance r, can be given in terms of an averaged version of the refractivity structure function of Eq. (30). In particular, it can be shown that we have [3]

$$D_{\theta;s}(r) = \left(\frac{2\pi}{\lambda}\right)^2 C^2 h^{8/3} D_s\left(\frac{r}{h}\right) \tag{32}$$

Here, λ denotes the wavelength of the carrier of the transmitted signal, h denotes the height of the turbulence (nominally 2 km), and $D_s(\alpha)$ is a spatial structure function given by

$$D_s(\alpha) = \frac{1}{\cos^2 \xi} \int_0^1 \int_0^1 \left\{ \widehat{D}_\chi\left[\sqrt{\alpha^2 + 2(x-y)\alpha \tan \xi + \left(\frac{x-y}{\cos \xi}\right)^2} \right] - \widehat{D}_\chi\left(\left| \frac{x-y}{\cos \xi}\right| \right) \right\} dx\, dy \tag{33}$$

where $\widehat{D}_\chi(\beta)$ is the *normalized* refractivity structure function [3] given in terms of the refractivity structure function of Eq. (30) as

$$\widehat{D}_\chi(\beta) \triangleq \frac{\beta^{2/3}}{1 + \left(\frac{\beta h}{L}\right)^{2/3}} = \frac{1}{C^2 h^{2/3}} D_\chi(\beta h) \tag{34}$$

It should be noted here that ξ is the zenith angle of the ray connecting the turbulence patch to the receive antennas as shown in Fig. 5.

From Eq. (31), the spatial autocorrelation of the atmospheric phase $R_{\theta;s}(r)$ is given by

$$R_{\theta;s}(r) = \frac{1}{2}\left[D_{\theta;s}(\infty) - D_{\theta;s}(r) \right]$$

Using Eq. (33), $R_{\theta;s}$ can be approximated as follows:

$$R_{\theta;s}(r) \approx \frac{1}{2}\left[\left(\frac{2\pi C h L^{1/3}}{\lambda \cos \xi}\right)^2 - D_{\theta;s}(r) \right] \tag{35}$$

Hence, using Eqs. (35), (32), (33), and (34), we can calculate the spatial correlations of the atmospheric phase processes for a fixed time.

A plot of $R_{\theta;s}(r)$ is shown in Fig. 6 for the following input parameters:

$$C = 2.4 \times 10^{-7} \text{ m}^{-1/3} \text{ (turbulence strength)}$$

$$h = 2 \text{ km (height of turbulence)}$$

$$L = 6 \text{ km (outer scale)}$$

$$F_c = 25 \text{ GHz (carrier frequency at Ka-band)}$$

$$\lambda = \frac{c}{F_c} = 0.012 \text{ m (wavelength)}$$

$$\xi = 0 \text{ (angle between turbulence patch and receive antennas measured from zenith)}$$

As can be seen, the phase is fairly correlated over large ranges of r. This is an expected and desired phenomenon, as it means that the phase perturbations seen by the receive antennas will not appear to be completely random.
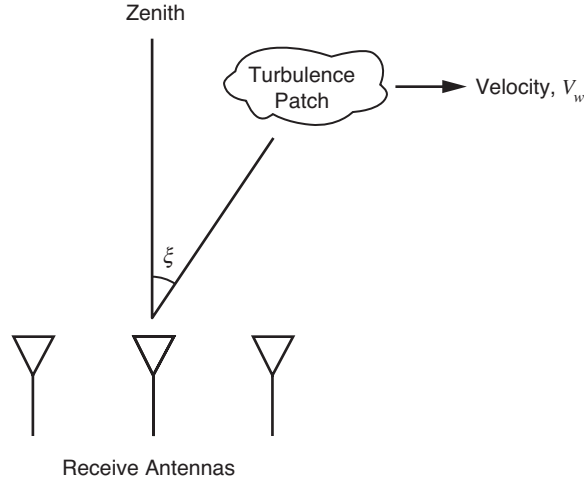

Fig. 5. Illustration of the position of the turbulence patch in relation to the receive antennas.
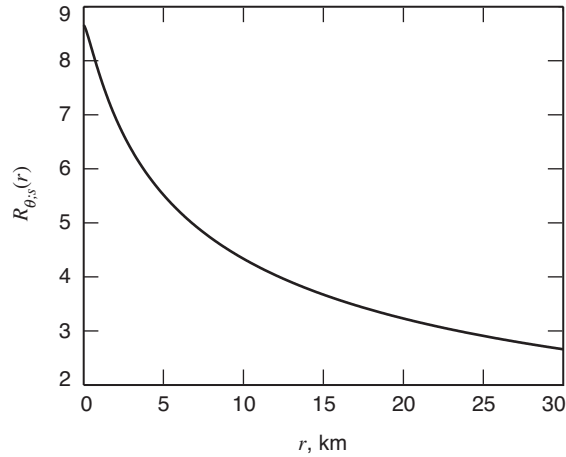

Fig. 6. Spatial autocorrelation of the atmospheric phase $R_{\theta;s}(r)$ as a function of distance r.

2. Temporal Correlation Model. In order to derive a temporal characterization of the atmospheric phase processes, typically a *frozen-screen* assumption [1,3] is made. According to this hypothesis, the spatial structure of the turbulence is assumed to be frozen in time. This assumption is approximately true for most turbulence patches (such as clouds) and is valid over relatively long periods of time [1].

Assuming in addition that the turbulence patch is moving at a velocity V_w (known as the *wind speed*) with respect to the receive antennas as in Fig. 5, it can be shown that we have [1,3]

$$D_{\theta;t}(\tau) = D_{\theta;s}(V_w\tau) \tag{36}$$

where $D_{\theta;s}(r)$ is the spatial phase structure function of Eq. (31) and $D_{\theta;t}(\tau)$ is the *temporal* structure function defined by

$$D_{\theta;t}(\tau) \triangleq E\left[|\theta_t(\tau_0 + \tau) - \theta_t(\tau_0)|^2\right] \tag{37}$$

From Eqs. (37), (36), and (31), it can be shown that we have

$$R_{\theta;t}(\tau) = R_{\theta;s}(V_w\tau) \tag{38}$$

where $R_{\theta;t}(\tau)$ is the temporal autocorrelation of the atmospheric phase. Hence, the temporal autocorrelation is simply a linearly stretched version of the spatial autocorrelation.

Using Eq. (35), $R_{\theta;t}(\tau)$ can be approximated as

$$R_{\theta;t}(\tau) \approx \frac{1}{2}\left[\left(\frac{2\pi ChL^{1/3}}{\lambda\cos\xi}\right)^2 - D_{\theta;s}(V_w\tau)\right] \tag{39}$$

where $D_{\theta;s}(r)$ is given by Eqs. (32) through (34).

A plot of $R_{\theta;t}(\tau)$ using the same input parameters as those used in Section III.A.1 is shown in Fig. 7 for various values of the wind speed V_w. As expected, as V_w increases, $R_{\theta;t}(\tau)$ becomes more compressed since the phase will appear more uncorrelated over time. In this case, this will make tracking more difficult since the received digital signal $\mathbf{x}[n]$ from Eq. (25) will change more rapidly. This difficulty in tracking will become more evident in Section V.

B. Obtaining a Jointly Spatio-Temporal Characterization of the Atmospheric Phase Processes

As stated before, although much of the literature on atmospheric phase modeling includes spatial and temporal statistical characterizations, there appears to be little to no work on joint characterizations. From this, we can infer that we can treat both effects in a *separable* way. In other words, we can treat spatial and temporal effects independently. This assumption clearly will not apply for heterogeneous turbulence patches, but for homogeneous ones in which the frozen-screen assumption holds, this model is physically plausible [1].

Mathematically, we model the autocorrelation function $\mathbf{R}_{\boldsymbol{\theta\theta}}(\tau)$ separably as follows:

$$\mathbf{R}_{\boldsymbol{\theta\theta}}(\tau) = \widehat{R}_{\theta;t}(\tau)\mathbf{R}_{\theta;s} \tag{40}$$
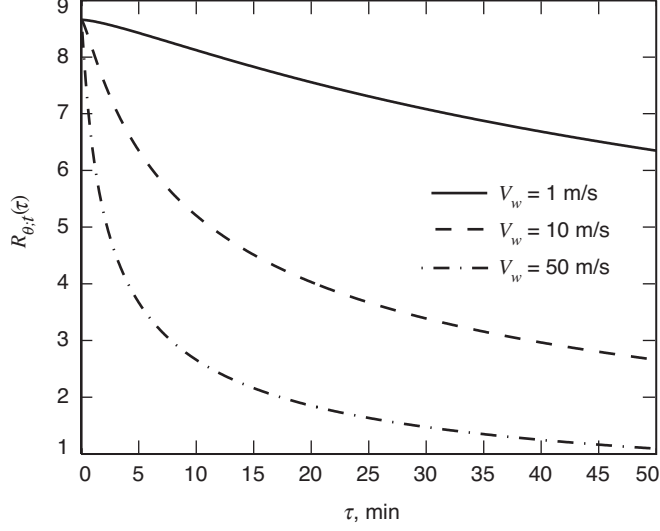
Fig. 7. Temporal autocorrelation of the atmospheric phase $R_{\theta;t}(\tau)$ as a function of time τ.

where $\widehat{R}_{\theta;t}(\tau)$ is a *normalized* version of the temporal autocorrelation function $R_{\theta;t}(\tau)$ from Eq. (39) and is given by

$$\widehat{R}_{\theta;t}(\tau) = \frac{R_{\theta;t}(\tau)}{R_{\theta;t}(0)} \tag{41}$$

Here, $\mathbf{R}_{\theta;s}$ is a constant matrix that depends only on the spatial autocorrelation function $R_{\theta;s}(r)$ from Eq. (35). In particular, we have

$$\mathbf{R}_{\theta;s} = \begin{bmatrix} R_{\theta;s}(r_{0,0}) & R_{\theta;s}(r_{0,1}) & \cdots & R_{\theta;s}(r_{0,N-1}) \\ R_{\theta;s}(r_{1,0}) & R_{\theta;s}(r_{1,1}) & \cdots & R_{\theta;s}(r_{1,N-1}) \\ \vdots & \vdots & \ddots & \vdots \\ R_{\theta;s}(r_{N-1,0}) & R_{\theta;s}(r_{N-1,1}) & \cdots & R_{\theta;s}(r_{N-1,N-1}) \end{bmatrix} \tag{42}$$

where $r_{k,\ell}$ represents the distance between the kth and ℓth receive antennas. As we have $r_{k,\ell} = r_{\ell,k}$ for all k, ℓ and $r_{k,k} = 0$ for all k, we can simplify Eq. (42) as follows:

$$\mathbf{R}_{\theta;s} = \begin{bmatrix} R_{\theta;s}(0) & R_{\theta;s}(r_{0,1}) & \cdots & R_{\theta;s}(r_{0,N-1}) \\ R_{\theta;s}(r_{0,1}) & R_{\theta;s}(0) & \cdots & R_{\theta;s}(r_{1,N-1}) \\ \vdots & \vdots & \ddots & \vdots \\ R_{\theta;s}(r_{0,N-1}) & R_{\theta;s}(r_{1,N-1}) & \cdots & R_{\theta;s}(0) \end{bmatrix}$$

Thus, $\mathbf{R}_{\theta;s}$ is a *Hermitian* matrix [4], as expected. For the special case in which we have a uniform linear array, $\mathbf{R}_{\theta;s}$ is also *Toeplitz* [4].

As can be seen from Eq. (40), $\mathbf{R}_{\theta\theta}(\tau)$ represents a model in which the spatial and temporal effects have been decoupled. The reason for normalizing the temporal autocorrelation as in Eq. (41) is to maintain consistency with the spatial autocorrelation model. Alternatively, we could have normalized the spatial

14

correlation matrix $\mathbf{R}_{\theta;s}$ by $R_{\theta;s}(0)$ to maintain consistency with the temporal autocorrelation model. As $R_{\theta;s}(0) = R_{\theta;t}(0)$ from Eq. (38), both approaches yield the same expression for $\mathbf{R}_{\boldsymbol{\theta\theta}}(\tau)$, as expected.

We now proceed to derive a discrete-time statistical model for the atmospheric phase processes based on uniform sampling of the continuous-time vector process $\boldsymbol{\theta}(t)$. There, we justify the approximation of the phase over a baud or symbol interval given in Eq. (19).

IV. Discrete-Time Statistical Model for the Sampled Atmospheric Phase Processes

A. Justifying the Sampled Phase Approximation

Prior to introducing a discrete-time statistical description of the atmospheric phase processes based on sampling, we must first justify the approximation from Eq. (19) that the atmospheric phases can be assumed to be constant over a baud interval. In order to measure the variation of $\theta_{k;a}(t)$ over time, we can use the following quantity:

$$P_k(\tau_0, \tau, \epsilon) \triangleq \Pr\left\{ |\theta_{k;a}(\tau_0 + \tau) - \theta_{k;a}(\tau_0)| \geq \epsilon \right\} \tag{43}$$

Here ϵ is a threshold value satisfying $\epsilon > 0$. Note that the quantity $P_k(\tau_0, \tau, \epsilon)$ is simply the probability that the magnitude of the difference of phases $\theta_{k;a}(\tau_0 + \tau)$ and $\theta_{k;a}(\tau_0)$ exceeds the threshold ϵ.

Although it is difficult to calculate $P_k(\tau_0, \tau, \epsilon)$ from Eq. (43) in closed form, it is fairly easy to compute an upper bound for it using *Chebyshev's inequality* [8]. Using Chebyshev's inequality on Eq. (43), we have

$$P_k(\tau_0, \tau, \epsilon) \leq \frac{E\left[|\theta_{k;a}(\tau_0 + \tau) - \theta_{k;a}(\tau_0)|^2\right]}{\epsilon^2} = \frac{D_{\theta;t}(\tau)}{\epsilon^2} = \frac{D_{\theta;s}(V_w\tau)}{\epsilon^2} \tag{44}$$

where we have used Eqs. (37) and (36) in Eq. (44).

Concerning Eq. (19), we are interested in studying the behavior of $P_k(\tau_0, \tau, \epsilon)$ for $\tau_0 = nT_s$ and $\tau \in [0, T_s)$. From Fig. 6, it can be seen that $R_{\theta;s}(r)$ is *monotonically decreasing* for $r \geq 0$. As we have $D_{\theta;s}(r) = 2\left[R_{\theta;s}(0) - R_{\theta;s}(r)\right]$ here by expanding Eq. (31), it follows that $D_{\theta;s}(r)$ is *monotonically increasing* for $r \geq 0$. From Eq. (44), this implies that we have

$$P_k(nT_s, \tau, \epsilon) \leq \frac{D_{\theta;s}(V_w\tau)}{\epsilon^2} < \frac{D_{\theta;s}(V_w T_s)}{\epsilon^2}, \ \forall \ \tau \in [0, T_s) \tag{45}$$

For a large wind speed of $V_w = 50$ m/s and a moderate sampling rate of $F_s = 1$ MHz (sampling interval of $T_s = 1$ μs), the probability that the phase changes by more than 1 degree (i.e., $\epsilon = \pi/180$) is *upper bounded* by 2.7535×10^{-4} using Eq. (45). Indeed this value is minute, and so we can say that with high probability the atmospheric phase is approximately constant over a sampling interval as in Eq. (19).

B. Statistical Properties of the Sampled Phase Processes

Recall that the discrete-time sampled phase processes $\beta_k[n]$ are defined as in Eq. (21). In this section, we characterize a statistical model for the discrete-time vector process $\boldsymbol{\beta}[n]$ defined below:

$$\boldsymbol{\beta}[n] \triangleq \begin{bmatrix} \beta_0[n] \\ \beta_1[n] \\ \vdots \\ \beta_{N-1}[n] \end{bmatrix}$$

Note that, from Eqs. (21) and (28), we have

$$\boldsymbol{\beta}[n] = \boldsymbol{\theta}(nT_s)$$

Since $\boldsymbol{\theta}(t)$ is a continuous-time WSS process, it can easily be shown [4] that $\boldsymbol{\beta}[n]$ is a discrete-time WSS process with

$$\boldsymbol{\mu_{\beta}} \triangleq E\big[\boldsymbol{\beta}[n]\big] = \boldsymbol{\mu_{\theta}}$$

$$\mathbf{R_{\beta\beta}}[k] \triangleq E\big[\boldsymbol{\beta}[n]\boldsymbol{\beta}^{\dagger}[n-k]\big] = \mathbf{R_{\theta\theta}}(kT_s) \tag{46}$$

As $\boldsymbol{\theta}(t)$ is assumed to be zero mean with autocorrelation as given in Eq. (40), we have

$$\boldsymbol{\mu_{\beta}} = \mathbf{0}\,, \ \ \mathbf{R_{\beta\beta}}[k] = \widehat{R}_{\theta;t}(kT_s)\,\mathbf{R}_{\theta;s} \tag{47}$$

1. Generating Instances of the Discrete-Time Atmospheric Phase Processes. To properly simulate the effects of the atmospheric phase perturbations on an adaptive array algorithm as is desired here, we need a way to generate instances of the atmospheric phase processes. The method used to generate these instances is similar to the one considered in [9]. In order to accomplish this, we need to characterize the *power spectral density* (psd) of $\boldsymbol{\beta}[n]$. This quantity is simply the *discrete-time* Fourier transform of $\mathbf{R_{\beta\beta}}[k]$ and is defined below [4]:

$$\mathbf{S_{\beta\beta}}(e^{j\omega}) \triangleq \sum_{k=-\infty}^{\infty} \mathbf{R_{\beta\beta}}[k]e^{-j\omega k}$$

If $\widehat{S}_{\theta;t}(j\Omega)$ denotes the *continuous-time* Fourier transform of $\widehat{R}_{\theta;t}(\tau)$, defined by

$$\widehat{S}_{\theta;t}(j\Omega) \triangleq \int_{-\infty}^{\infty} \widehat{R}_{\theta;t}(\tau)e^{-j\Omega\tau}\,d\tau$$

then from Eq. (47), it can be shown [4] that $\mathbf{S_{\beta\beta}}(e^{j\omega})$ is given by

$$\mathbf{S_{\beta\beta}}(e^{j\omega}) = \underbrace{\left[\frac{1}{T_s} \sum_{\ell=-\infty}^{\infty} \widehat{S}_{\theta;t}\left(j\left(\frac{\omega - 2\pi\ell}{T_s}\right)\right)\right]}_{P(e^{j\omega})} \mathbf{R}_{\theta;s} \tag{48}$$

where $P(e^{j\omega})$ is the *aliased* spectrum of $\widehat{R}_{\theta;t}(\tau)$ obtained due to uniform sampling at $\tau = kT_s$.

Since $\widehat{S}_{\theta;t}(j\Omega)$ is the continuous-time Fourier transform of a valid autocorrelation function $\widehat{R}_{\theta;t}(\tau)$, it follows that $\widehat{S}_{\theta;t}(j\Omega)$ is a valid continuous-time psd, meaning $\widehat{S}_{\theta;t}(j\Omega) \geq 0$ for all Ω. From Eq. (48), we clearly have $P(e^{j\omega}) \geq 0$ for all ω, and so $P(e^{j\omega})$ is a valid discrete-time psd, as expected. Hence, it can be factored as

$$P(e^{j\omega}) = \left|Q(e^{j\omega})\right|^2 \tag{49}$$

where $Q(e^{j\omega})$ is some *spectral factor* [4] of $P(e^{j\omega})$.

Analogously, it can be shown that the Hermitian matrix $\mathbf{R}_{\theta;s}$ from Eq. (42) is *positive semidefinite* [4], meaning that $\mathbf{v}^{\dagger}\mathbf{R}_{\theta;s}\mathbf{v} \geq 0$ for all vectors $\mathbf{v} \neq \mathbf{0}$. Hence, it can be factored as follows [4]:

$$\mathbf{R}_{\theta;s} = \mathbf{T}\mathbf{T}^{\dagger} \tag{50}$$

Here $\mathbf{T}$ is some *matrix spectral factor* of $\mathbf{R}_{\theta;s}$.

Combining Eqs. (49) and (50) with Eq. (48), it follows that the psd $\mathbf{S}_{\boldsymbol{\beta}\boldsymbol{\beta}}(e^{j\omega})$ can be expressed as follows:

$$\mathbf{S}_{\boldsymbol{\beta}\boldsymbol{\beta}}(e^{j\omega}) = \left|Q(e^{j\omega})\right|^2 \mathbf{T}\mathbf{T}^{\dagger} = Q(e^{j\omega})\mathbf{T}\mathbf{T}^{\dagger}Q^*(e^{j\omega}) = \left(\mathbf{T}Q(e^{j\omega})\right)\left(\mathbf{T}Q(e^{j\omega})\right)^{\dagger} \tag{51}$$

Note that Eq. (51) is a spectral factor decomposition of the psd $\mathbf{S}_{\boldsymbol{\beta}\boldsymbol{\beta}}(e^{j\omega})$.

In order to generate instances of the colored process $\boldsymbol{\beta}[n]$, we can process an uncorrelated white WSS process $\boldsymbol{\psi}[n]$ (with $\boldsymbol{\mu}_{\boldsymbol{\psi}} = \mathbf{0}$ and $\mathbf{S}_{\boldsymbol{\psi}\boldsymbol{\psi}}(z) = \mathbf{I}$) through a spectral factor of $\mathbf{S}_{\boldsymbol{\beta}\boldsymbol{\beta}}(e^{j\omega})$ as given in Eq. (51). If we have

$$\boldsymbol{\psi}[n] \triangleq \begin{bmatrix} \psi_0[n] \\ \psi_1[n] \\ \vdots \\ \psi_{N-1}[n] \end{bmatrix}$$

then $\boldsymbol{\beta}[n]$ can be generated as shown in Fig. 8.

A few comments are in order here. First, as the phase perturbations are attributed to cumulative effects from the atmosphere, we model the distribution of the phases $\{\beta_k[n]\}$ to be *Gaussian* [1]. This means that the white process $\boldsymbol{\psi}[n]$ leading to $\boldsymbol{\beta}[n]$ as in Fig. 8 should also be Gaussian.

In addition to modeling the distribution of the phases, we must also consider the implementation of the temporal coloring filter $Q(z)$. Here, we model $Q(z)$ as a stable Mth-order *autoregressive* (AR) approximation [8] to a spectral factor of $P(e^{j\omega})$ as in Eq. (49). This means that $Q(z)$ is implemented as
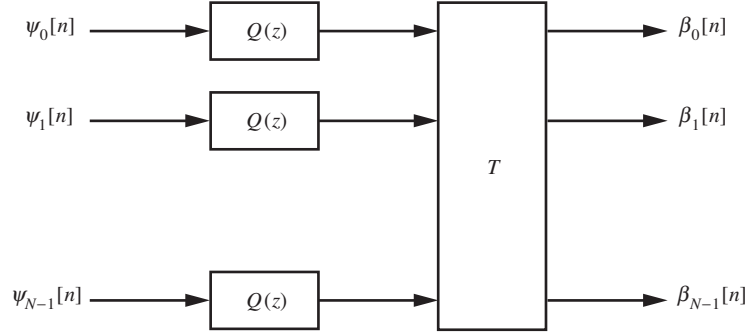
$$Q(z) = \frac{1}{A(z)}$$

Fig. 8. System used to generate instances of the colored process $\beta[n]$ from the uncorrelated white process $\psi[n]$.

where $A(z)$ is an Mth-order polynomial in z^{-1}. For the sake of stability, the zeros of $A(z)$ are constrained to the region $\{z : |z| < 1\}$ (i.e., inside the unit circle) [4]. The coefficients of $A(z)$ can be found efficiently using the Levinson–Durbin recursion algorithm [8].[5]

Sample realizations of the discrete-time atmospheric phase processes seen for a three-element uniform linear array are shown in Fig. 9 for a spacing of $d = 50$ m between the array elements. The atmospheric input parameters used were the same as those in Section III.A.1 with a wind speed of $V_w = 10$ m/s. Also, the order of the AR model used was $M = 30$. As can be seen, the phases appear to be strongly spatially and temporally correlated.

The reason for such a strong temporal correlation is the high sampling rate (equivalently small sampling interval) used. Here, we used $F_s = 1$ MHz, corresponding to a sampling interval of $T_s = 1$ μs, even though from Fig. 7 it can be seen that the phases typically are significantly correlated over several *minutes*.

A plot of the time dependence of a sample realization of one of the phases considered above is shown in Fig. 10. As can be seen, the phase changes appreciably only after a long enough time (on the order of several seconds). This suggests that the nonstationarity caused by the atmospheric phase perturbations is small and should be able to be tracked sufficiently well. In the next section, this will be shown to be the case with respect to the SMI algorithm.

V. Acquisition Simulation Results Using the SMI Algorithm

Given the signals appearing at the receive antennas [equivalently the vector signal $\mathbf{x}[n]$ from Eq. (25)], we would like to obtain the desired scalar data sequence $d[n]$. In order to help accomplish this, the signals are typically *combined* using a linear time-varying multiple input–single output (MISO) system as shown in Fig. 11. Here $\mathbf{w}^{\dagger}[m, n]$ is the time-varying impulse response of the system[6] (i.e., $\mathbf{w}^{\dagger}[n - m, n]$ is the response to the input δ_{n-m}) and is $1 \times N$. The impetus for combining the signals in this way is to attempt to coherently add up the diversified versions of the desired signal $d[n]$ as seen by the various receive antennas.

---

[5] In [9], $Q(z)$ was modeled as a *moving average* (MA) approximation to a spectral factor of $P(e^{j\omega})$, meaning that $Q(z)$ was itself implemented as a polynomial in z^{-1}. This model, however, is unable to capture the non-negligible long-term temporal correlations that an AR model can, unless the length of the MA filter is made long enough. Making the length of the MA model long enough, however, is not feasible for large array simulations due to memory and computation time limitations.

[6] The MISO impulse response is defined using the dagger † transpose conjugate notation to make the output $y[n]$ resemble the inner product of the $N \times 1$ system $\mathbf{w}[m, n]$ and the shifted input $\mathbf{x}[n - m]$. This is nothing more than a notational convention typically used in antenna array processing.
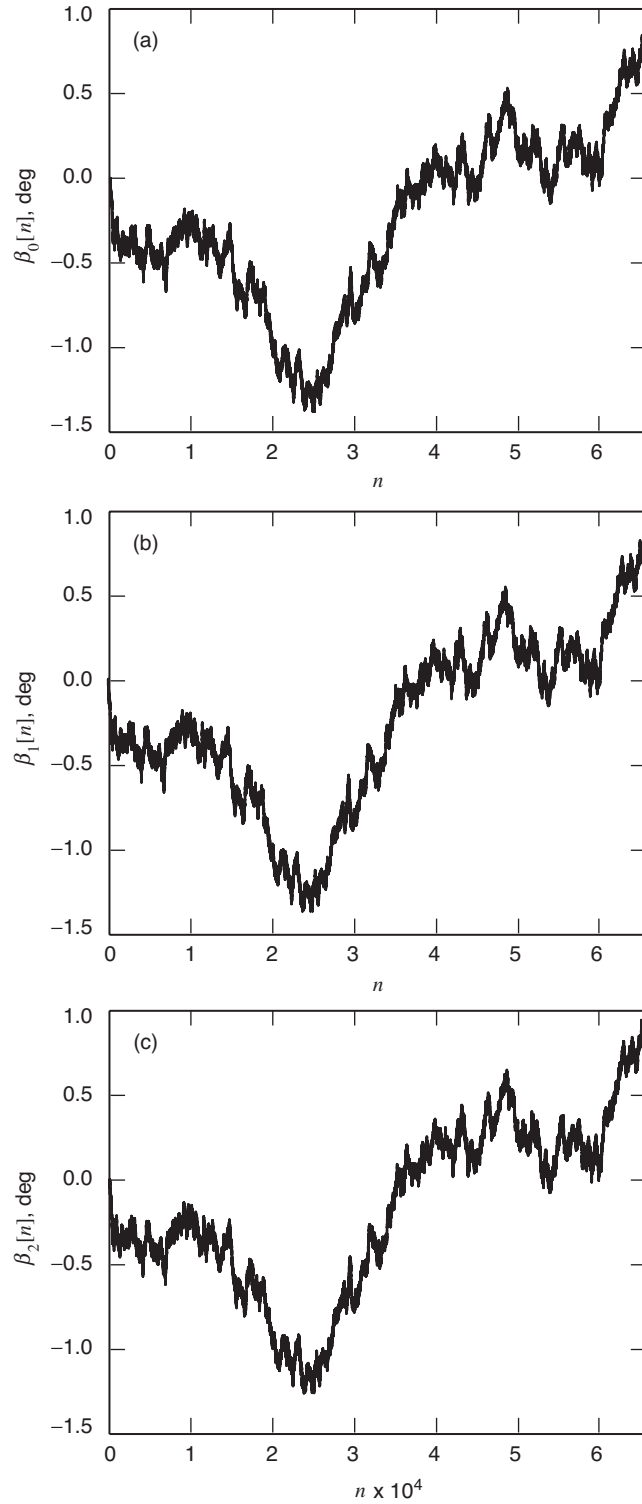
Fig. 9. Sample realizations of the discrete-time atmospheric phase processes for a three-element uniform linear array with a spacing of $d = 50$ m between the receive antennas: (a) first element, (b) second element, and (c) third element.
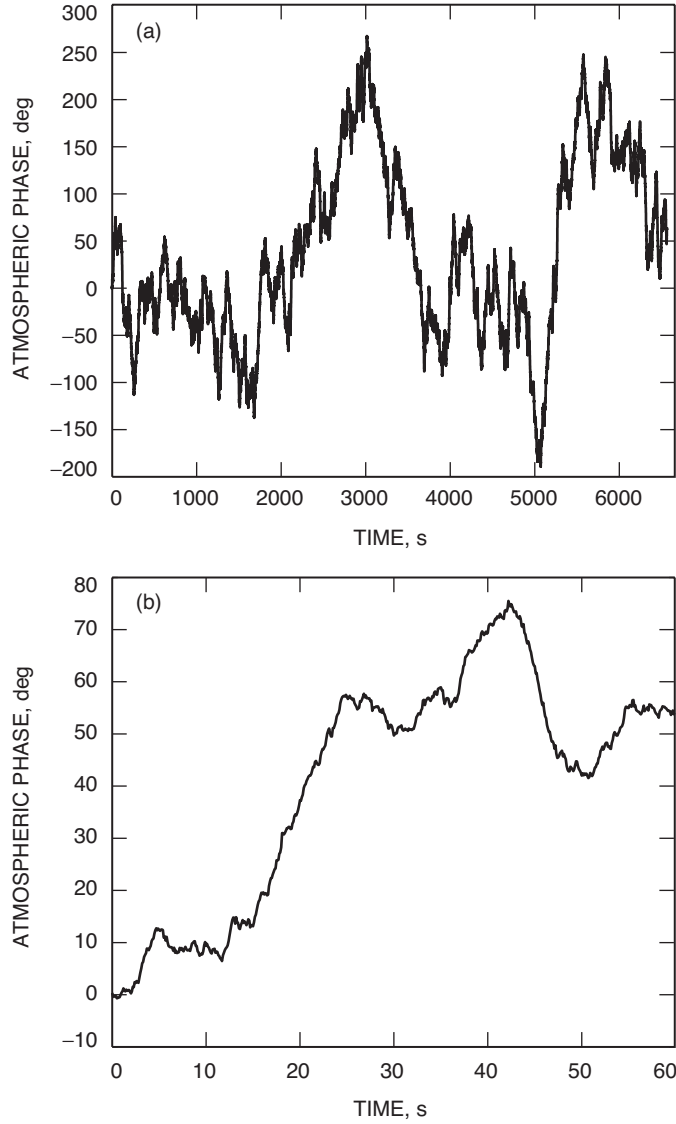
Fig. 10. Sample realization of an atmospheric phase
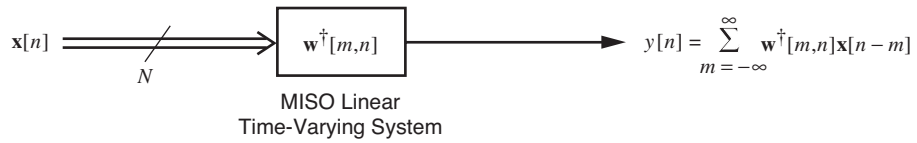process over (a) a large time scale and (b) a minute.

Fig. 11. Linear time-varying MISO system used to combine the antenna array outputs.

For most narrowband applications, $\mathbf{w}^\dagger[m,n]$ is chosen to be a *memoryless* system [4] in which we have

$$\mathbf{w}^\dagger[m,n] = \begin{cases} \mathbf{w}^\dagger[n], & m = 0 \\ \mathbf{0}, & m \neq 0 \end{cases} = \mathbf{w}^\dagger[n]\delta_m$$

In this case, we have

$$y[n] = \mathbf{w}^\dagger[n]\mathbf{x}[n] \tag{52}$$

and the resulting system is memoryless in that the output is only a linear combination of the elements of the current input $\mathbf{x}[n]$ and not of past or future samples.

A. Minimum Mean-Squared Error Combiner (Wiener Filter)

For the purpose of acquisition, a known reference signal $d_r[n]$ often is transmitted so that the receiver can "phase up" to this reference. In other words, the signal combiner $\mathbf{w}[n]$ is chosen to make the output $y[n] = \mathbf{w}^\dagger[n]\mathbf{x}[n]$ as close to the desired reference signal $d_r[n]$ as possible. For example, the *Wiener filter* $\mathbf{w}_o[n]$ [2] minimizes the mean-squared error between the output $y[n]$ and reference $d_r[n]$ given by

$$\xi[n] \triangleq E\left[|y[n] - d_r[n]|^2\right] \tag{53}$$

It can easily be shown [2] that the Wiener filter $\mathbf{w}_o[n]$ can be expressed in closed form in terms of a matrix inverse as follows:

$$\mathbf{w}_o[n] = \mathcal{R}_{\mathbf{xx}}^{-1}[n]\mathcal{R}_{\mathbf{x}d_r}[n] \tag{54}$$

where we have[7]

$$\mathcal{R}_{\mathbf{xx}}[n] \triangleq E\left[\mathbf{x}[n]\mathbf{x}^\dagger[n]\right] \tag{55}$$

$$\mathcal{R}_{\mathbf{x}d_r}[n] \triangleq E\left[\mathbf{x}[n]d_r^*[n]\right] \tag{56}$$

We should note that we assumed a priori that $\mathcal{R}_{\mathbf{xx}}[n]$ is invertible in arriving at Eq. (54), which in practice typically will be the case. If it is not, however, then the matrix inverse in Eq. (54) should be replaced with a pseudoinverse.

The corresponding optimal mean-squared error $\xi_o[n]$ is given below as follows [2]:

$$\xi_o[n] = \sigma_{d_r}^2[n] - \mathcal{R}_{\mathbf{x}d_r}^\dagger[n]\mathcal{R}_{\mathbf{xx}}^{-1}[n]\mathcal{R}_{\mathbf{x}d_r}[n] \tag{57}$$

where $\sigma_{d_r}^2[n]$ is given by $\sigma_{d_r}^2[n] = E\left[|d_r[n]|^2\right]$. At this point, a few comments are in order.

---

[7] We use a calligraphic font for correlation matrices/vectors here to distinguish the time dependence of these possibly nonstationary quantities from the lag dependence of WSS correlations such as the one in Eq. (46).

First, note that the behavior of $\xi_o[n]$ as a function of n can be used to gauge the joint stationarity of $\mathbf{x}[n]$ and $d_r[n]$. The reason for this is that if $\mathbf{x}[n]$ and $d_r[n]$ are jointly WSS, then $\xi_o[n]$ is a constant. Heuristically, it can be argued that the more $\xi_o[n]$ varies with n, the less jointly stationary $\mathbf{x}[n]$ and $d_r[n]$ appear to be. We will investigate this stationarity more in detail via simulations later on in this section.

Secondly, it should be noted that in the case in which the received signal $\mathbf{x}[n]$ consists of a linearly scaled version of $d_r[n]$ corrupted by an uncorrelated additive white noise, the Wiener filter $\mathbf{w}_o[n]$ is optimal not only for minimizing the mean-squared error but also for maximizing the output SNR [2]. Although this will only be approximately true in the case in which the atmospheric phase effects are included, we will nonetheless still assume this to be the case when we consider the *combining loss* of the SMI algorithm, which is defined later on in this section.

B. The Sample Matrix Inversion (SMI) Algorithm

Although the Wiener filter is optimal for minimizing the mean-squared error of the output signal, it requires knowledge of the second-order statistics of the received signal $\mathbf{x}[n]$ (as well as the joint statistics of $\mathbf{x}[n]$ and $d_r[n]$). As this typically will not be known in practice, we instead *estimate* these statistics based on actual observed data. This estimation leads to the *sample matrix inversion* (SMI) algorithm that we will use here to phase up to the reference signal.

Suppose that we have a block of K consecutive samples of $\mathbf{x}[n]$ from $\mathbf{x}[n-K]$ to $\mathbf{x}[n-1]$ that were obtained independently of each other. To estimate the quantities $\mathcal{R}_{\mathbf{xx}}[n]$ and $\mathcal{R}_{\mathbf{x}d_r}[n]$ from Eqs. (55) and (56), respectively, we use the *sample mean* of each of these quantities given below:

$$\widehat{\mathcal{R}}_{\mathbf{xx};K}[n] \triangleq \frac{1}{K} \sum_{k=1}^{K} \mathbf{x}[n-k]\mathbf{x}^{\dagger}[n-k] \tag{58}$$

$$\widehat{\mathcal{R}}_{\mathbf{x}d_r;K}[n] \triangleq \frac{1}{K} \sum_{k=1}^{K} \mathbf{x}[n-k]d_r^{*}[n-k] \tag{59}$$

If $\mathbf{x}[n-K], \cdots, \mathbf{x}[n-1]$ and $d_r[n-K], \cdots, d_r[n-1]$ are jointly Gaussian, then the sample mean quantities of Eqs. (58) and (59) can be shown to be ML estimates of Eqs. (55) and (56), respectively [8].

With the sample estimates of $\mathcal{R}_{\mathbf{xx}}[n]$ and $\mathcal{R}_{\mathbf{x}d_r}[n]$ given in Eqs. (58) and (59), we can estimate the Wiener filter of Eq. (54) as follows:

$$\widehat{\mathbf{w}}[n] = \widehat{\mathcal{R}}_{\mathbf{xx};(n-n_0)+K_0}^{-1}[n]\widehat{\mathcal{R}}_{\mathbf{x}d_r;(n-n_0)+K_0}[n], \; n \geq n_0 \tag{60}$$

Here, n_0 represents a starting time to initiate the signal combining and K_0 represents the block length to be used initially at $n = n_0$.

A few comments are in order at this point. First note that, as time increases, the block length $K = (n-n_0) + K_0$ of samples used to form the correlation estimates increases as well. Intuitively, we might expect that, as we collect more samples, the combining vector $\widehat{\mathbf{w}}[n]$ will approach the optimal Wiener filter $\mathbf{w}_o[n]$. Although this indeed is true when $\mathbf{x}[n]$ and $d_r[n]$ are jointly WSS [2] (in which case $\mathbf{w}_o[n]$ is actually a constant vector), this may not be the case when they are not. For example, if $\mathbf{x}[n]$ fluctuates rapidly in time, it may be more advantageous to fix the block size at a small value in order to better capture the localized variations of the signal statistics.

In addition to this issue, we must also exercise caution in the choice of the initial block size K_0. As $\widehat{\mathcal{R}}_{\mathbf{xx};K}[n]$ from Eq. (58) is a sum of K dyadic terms (i.e., terms of the form $\mathbf{vv}^\dagger$ for some vector $\mathbf{v}$), we must have $K \geq N$ in order for $\widehat{\mathcal{R}}_{\mathbf{xx};K}[n]$ to be invertible [4]. Alternatively, we can replace the matrix inverse in Eq. (60) with a pseudoinverse; however, as shown in the next section, the tracking performance is poor for such small values of block lengths.

The method used to obtain the combining weight of Eq. (60) is formally the SMI algorithm. Although this method is computationally complex in that it requires the computation of a matrix inverse, this is mitigated by the fact that we can use the *matrix inversion lemma* [4] to obtain the new inverse given the previously computed one. We can also slightly reduce the complexity by removing the scaling factor of $1/K$ present in Eqs. (58) and (59), as they cancel each other out in Eq. (60).

C. Performance Metrics for Acquisition Evaluation

In order to properly evaluate the acquisitioning ability of the SMI algorithm, we need a way to measure the performance of the SMI algorithm with respect to the mean-squared error optimal Wiener solution. Here, we will consider two such metrics, namely the *misalignment* and the *combining loss*, which we review below.

1. Misalignment. As the Wiener filter $\mathbf{w}_o[n]$ is optimal in the mean-squared sense, clearly any other combining weight vector $\mathbf{w}[n]$ will necessarily yield at least as large a mean-squared error as $\mathbf{w}_o[n]$. One way to measure the performance of some combining weight with respect to the Wiener solution is to compute the *excess* mean-squared error, which is the difference between the mean-squared error of the combining weight under consideration and that of the Wiener filter. A normalized variant of this, known as the *misalignment*, is defined below [2]:

$$\mu[n] \triangleq \frac{\xi[n] - \xi_o[n]}{\xi_o[n]} = \frac{\xi[n]}{\xi_o[n]} - 1 \tag{61}$$

where $\xi[n]$ is the mean-squared error of Eq. (53) corresponding to some combining weight vector $\mathbf{w}[n]$ and $\xi_o[n]$ is the mean-squared error of the Wiener filter $\mathbf{w}_o[n]$ as given in Eq. (57).

As $\xi[n] \geq \xi_o[n]$, clearly $\mu[n] \geq 0$ with equality if $\mathbf{w}[n]$ is the Wiener filter $\mathbf{w}_o[n]$. Note that because of this property $\mu[n]$ is a measure of how well an adaptive algorithm can track the Wiener solution. If $\mu[n]$ is large, then the algorithm is performing poorly compared to the Wiener solution, whereas if $\mu[n]$ is small (i.e., close to 0), then the algorithm is performing well. For the case in which the input $\mathbf{x}[n]$ and reference signal $d_r[n]$ are jointly WSS (in which case $\mathbf{w}_o[n]$ becomes a constant vector), the SMI and *least mean squares* (LMS) algorithms can be shown to yield $\mu[n] \to 0$ as $n \to 0$ [2,10]. Furthermore, in this case, the misalignment of the SMI algorithm converges *monotonically* to 0 [10].

2. Combining Loss. As stated above, in the case in which $\mathbf{x}[n]$ consists of a linearly scaled version of the reference signal $d_r[n]$ along with an additive white noise component, the Wiener solution is optimal not only for minimizing the mean-squared error but also for maximizing the output SNR [2]. Though this will only approximately be true when we include the effects due to the atmospheric phases, nevertheless it is worthwhile to compare the output SNR of some combining weight vector $\mathbf{w}[n]$ with that of the Wiener filter $\mathbf{w}_o[n]$.

Prior to introducing such a measure, we must first properly define what is meant by output SNR in this setting. Consider the received signal $\mathbf{x}[n]$ from Eq. (25) when the reference signal $d_r[n]$ is transmitted (i.e., $d[n] = d_r[n]$). This can be expressed as

$$\mathbf{x}[n] = \mathbf{s}[n] + \mathbf{v}[n]$$

where $\mathbf{s}[n] = \mathbf{B}[n]\mathbf{a}d_r[n]$ is the *signal* component of $\mathbf{x}[n]$ and $\mathbf{v}[n]$ is the *noise* component. Upon combining the receive antenna inputs using the weight vector $\mathbf{w}[n]$ as in Eq. (52), we obtain the output $y[n]$, which can be decomposed as

$$y[n] = y_{\mathbf{s};\mathbf{w}}[n] + y_{\mathbf{v};\mathbf{w}}[n]$$

where $y_{\mathbf{s};\mathbf{w}}[n] = \mathbf{w}^{\dagger}[n]\mathbf{s}[n]$ is the output signal component of $y[n]$ and $y_{\mathbf{v};\mathbf{w}}[n] = \mathbf{w}^{\dagger}[n]\mathbf{v}[n]$ is the output noise component. Formally, in the spirit of Eq. (26), we define the output SNR as follows:

$$\mathrm{SNR}_{y;\mathbf{w}}[n] \triangleq \frac{E\left[|y_{\mathbf{s};\mathbf{w}}[n]|^2\right]}{E\left[|y_{\mathbf{v};\mathbf{w}}[n]|^2\right]}$$

With this definition of output SNR, the *combining loss* is simply a measure of the output SNR of some combining weight $\mathbf{w}[n]$ compared with that of the Wiener solution $\mathbf{w}_o[n]$. In particular, the combining loss $\mathcal{L}[n]$ is simply a measure of the difference between these two output SNRs in decibels (dB), as given below:

$$\mathcal{L}[n] \triangleq 10\log_{10}\left(\frac{\mathrm{SNR}_{y;\mathbf{w}}[n]}{\mathrm{SNR}_{y;\mathbf{w}_o}[n]}\right) = 10\log_{10}\left(\mathrm{SNR}_{y;\mathbf{w}}[n]\right) - 10\log_{10}\left(\mathrm{SNR}_{y;\mathbf{w}_o}[n]\right)$$

$$= \mathrm{SNR}_{y;\mathbf{w}}[n] \; (\mathrm{dB}) - \mathrm{SNR}_{y;\mathbf{w}_o}[n] \; (\mathrm{dB}) \tag{62}$$

For the case in which $\mathbf{x}[n]$ and $d_r[n]$ are jointly WSS and $\mathbf{v}[n]$ is an AWGN process, the SMI algorithm can be shown to have a combining loss that monotonically converges to 0 as $n \to \infty$ [10].

D. Simulation Results in the Presence of Atmospheric Phase Effects

At this point, it is worthwhile to analyze the effects due to the atmospheric phase perturbations on the stationarity of the received signal $\mathbf{x}[n]$ as well as the combining performance achievable using the SMI algorithm for acquisition. To gauge the stationarity of $\mathbf{x}[n]$, we will consider the Wiener mean-squared error $\xi_o[n]$ from Eq. (57), whereas to measure the combining performance of the SMI algorithm, we will consider both the misalignment $\mu[n]$ from Eq. (61) as well as the combining loss $\mathcal{L}[n]$ from Eq. (62).

For the atmospheric phases, suppose that we use the same parameters as those in Section III.A.1. Furthermore, suppose that the wind speed V_w is set at a typical value of 10 m/s and that a 30th-order (i.e., $M = 30$) AR model was used to simulate the temporal correlation of the atmospheric phases.

For the purpose of simulation, we opted to vary the sampling rate (equivalently the baud rate in this case as well) over the two values $F_s = 0.1$ kHz and 1.0 kHz, corresponding to sampling intervals of $T_s = 10$ ms and $T_s = 1$ ms, respectively. The reason for this choice of low sampling rates is that the effects due to the resulting nonstationarity of the received signal caused by the atmospheric phase effects become more pronounced at lower rates.

In all of the simulations considered here, we opted to use a pure tone reference coming to the antenna array at zenith. Here, the gain factors of both the reference and geometric array vector were set to unity for simplicity. In other words, we chose

$$d_r[n] = 1 \quad \forall \; n$$

$$\mathbf{a} = \begin{bmatrix} 1 & 1 & \cdots & 1 \end{bmatrix}^T$$

Here, the array used was a uniform linear array with an inter-element spacing of $d = 50$ m. The number of receive antennas was chosen to be a moderate value of $N = 50$ here to help motivate the use of ultra-large arrays (ULAs) for interferometry in the DSN. Also, the gain factor A and noise variance σ^2 were chosen such that the input SNR of Eq. (26) was set to -5 dB. The reason for this choice of input SNR is motivated by the requirements of turbo/low-density parity-check (LDPC) codes expected to be implemented in the DSN array system.

For the SMI algorithm, the starting time and initial block length were chosen to be $n_0 = 0$ and $K_0 = 0$, respectively. In the special case for which the block size was zero, the correlation matrices required for the SMI algorithm were initialized to zero. Finally, the number of ensemble realizations of $\mathbf{x}[n]$ for each n in all of the simulations was set at 8,192.

In Fig. 12, we have plotted the observed mean-squared error $\xi_o[n]$ for the Wiener filter as given in Eq. (57) for the values of F_s as mentioned above. Furthermore, we have included the results obtained for the stationary case of no atmospheric phase effects. As can be seen, the error varied the most for the smallest sampling rate (largest sampling interval) and varied less for the largest sampling rate (smallest sampling interval). This is consistent with our intuition that the received signal $\mathbf{x}[n]$ should be less stationary the more the atmospheric phases change. The longer the sampling interval, the longer the atmospheric phases have to change by a significant amount from sample to sample.

In Fig. 13, we have plotted the observed misalignment $\mu[n]$ from Eq. (61) for each of the sampling rates F_s from above. As before, we have included the misalignment for the stationary case of no atmospheric phase effects. From the plot, it can be seen that the misalignment in all cases reached a maximum value at $n = 50$, which corresponds to the case at which the block length K used in the SMI algorithm equals the number of antennas N. This is the value of the block length at which the matrix $\widehat{\tilde{\mathcal{R}}}_{\mathbf{xx};K}[n]$ from Eq. (58) becomes invertible. At block lengths smaller than N, $\widehat{\mathcal{R}}_{\mathbf{xx};K}[n]$ is necessarily singular [4], whereas for block lengths greater than or equal to N, $\widehat{\mathcal{R}}_{\mathbf{xx};K}[n]$ is most likely invertible due to the randomness of the input $\mathbf{x}[n]$. The degradation seen when $K = N$ is consistent with the theoretical results obtained by Reed et al. [10] for the case of no atmospheric phase perturbations.

From Fig. 13, it also can be seen that, for $n > N$, the misalignment steadily decreased in all cases and came close to zero in all cases as well, suggesting that the SMI algorithm yielded a performance close to the Wiener solution. However, it can be seen that the misalignment for $F_s = 0.1$ kHz was on average greater than that for $F_s = 1.0$ kHz, suggesting that the increased nonstationarity due to the atmospheric phase effects made tracking the optimal Wiener solution somewhat more difficult.

Finally, in Fig. 14, we have plotted the observed combining loss $\mathcal{L}[n]$ from Eq. (62). As with the misalignment, it can be seen that the most noticeable degradation occurred for $n = N$, as expected from the theoretical analysis of [10]. For $n > N$, it can be seen that the performance steadily improved and the loss approached zero as n increased for both sampling rates considered as well as for the stationary input case. This suggests that the SMI algorithm is performing like the Wiener filter in terms of output SNR as the block length continues to increase. As with the misalignment, the combining loss for $F_s = 0.1$ kHz was on average slightly worse than for $F_s = 1.0$ kHz, suggesting that the nonstationarity imparted by the atmospheric phases became more pronounced for $F_s = 0.1$ kHz than for $F_s = 1.0$ kHz.
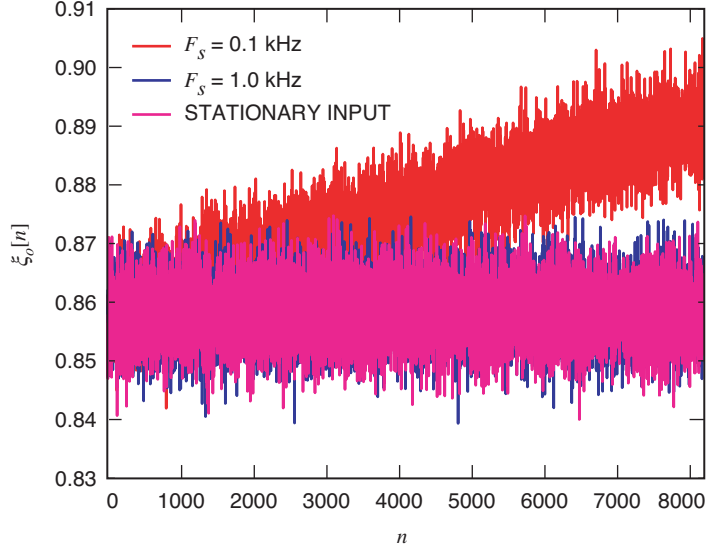
Fig. 12. Observed mean-squared error $\xi_o[n]$ for the Wiener filter for various sampling rates. (Results for a WSS input corresponding to no atmospheric phase effects included for comparison.)
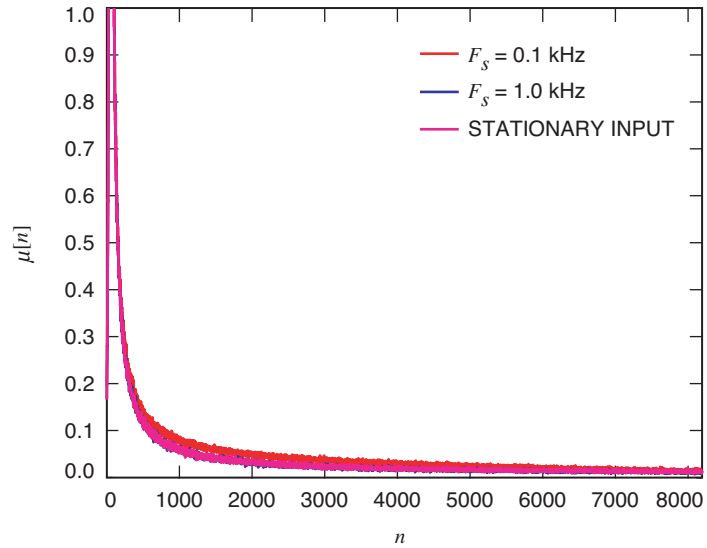

Fig. 13. Observed misalignment $\mu[n]$ for various sampling rates. (Results for a WSS input corresponding to no atmospheric phase effects included for comparison.)

VI. Concluding Remarks

In this article, we proposed a joint spatial/temporal statistical model for the atmospheric phase perturbation processes seen at the receiver end of an antenna array system such as that used in the DSN. Based on this continuous-time model, we formulated a corresponding discrete-time model based on uniform sampling of the continuous-time process. The impetus for considering such a description arises in a digital communications setting in which sampling is ubiquitously employed.
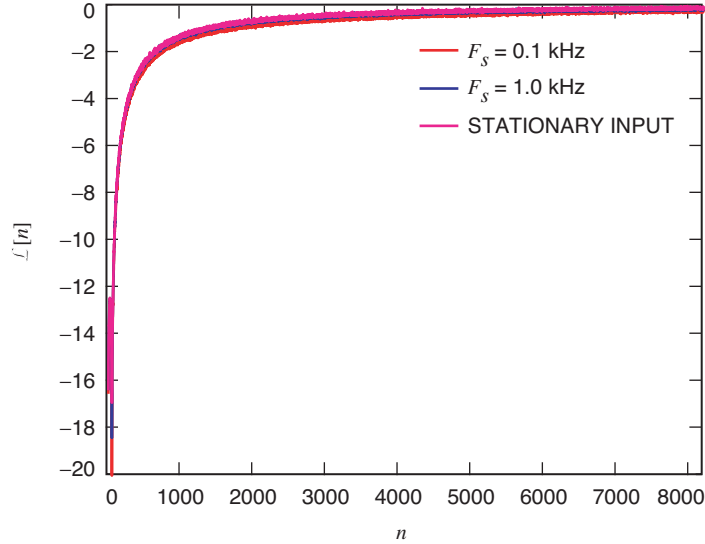
Fig. 14. Observed combining loss $\mathcal{L}[n]$ for various sampling rates. (Results for a WSS input corresponding to no atmospheric phase effects included for comparison.)

With this discrete-time characterization in place, we analyzed the effects of the atmospheric phase perturbations on the acquisition performance of the SMI algorithm for combining the array outputs. Through simulations, it was shown that the nonstationarity imparted by the atmospheric phases was relatively mild for the sampling rates considered. This implies that the SMI algorithm is adequate for use to phase up the array outputs to a desired reference signal in these cases.

Although the effects due to the atmosphere were shown to be minor for the moderate number of receive antennas used in the simulations here, it is not clear at this time how much the atmosphere will affect the acquisition performance when we consider a large number of antennas, such as those expected to be used in ultra-large arrays (ULAs). In such systems, the perturbations in phase due to the atmosphere are expected to be more pronounced because phases at antennas farther away from each other will be more weakly correlated, both in space and in time. These effects are the subject of ongoing research.

References

[1] A. R. Thompson, J. M. Moran, and G. W. Swenson, Jr., *Interferometry and Synthesis in Radio Astronomy*, 2nd ed., New York: John Wiley & Sons, Inc., 2001.

[2] A. H. Sayed, *Fundamentals of Adaptive Filtering*, Hoboken, New Jersey: John Wiley & Sons, Inc., 2003.

[3] R. N. Treuhaft and G. E. Lanyi, "The Effect of the Dynamic Wet Troposphere on Radio Interferometric Measurements," *Radio Science*, vol. 22-2, pp. 251–265, March/April 1987.

[4] P. P. Vaidyanathan, *Multirate Systems and Filter Banks*, Englewood Cliffs, New Jersey, Prentice Hall PTR, 1993.

[5] D. Tse and P. Viswanath, *Fundamentals of Wireless Communication*, New York: Cambridge University Press, 2005.

[6] M. K. Simon, S. M. Hinedi, and W. C. Lindsey, *Digital Communications Techniques: Signal Design and Detection*, Upper Saddle River, New Jersey: Prentice Hall PTR, 1994.

[7] C. L. Carilli and M. A. Holdaway, "Tropospheric Phase Calibration in Millimeter Interferometry," *Radio Science*, vol. 34-4, pp. 817–840, July/August 1999,

[8] A. Papoulis and S. U. Pillai, *Probability, Random Variables and Stochastic Processes*, New York: McGraw-Hill, 2002.

[9] C. H. Lee, V. Vilnrotter, E. Satorius, Z. Ye, D. Fort, and K.-M. Cheung, "Large-Array Signal Processing for Deep-Space Applications," *The Interplanetary Network Progress Report 42-150, April–June 2002*, Jet Propulsion Laboratory, Pasadena, California, pp. 1–28, August 15, 2002.
http://ipnpr/progress_report/42-150/150I.pdf

[10] I. S. Reed, J. D. Mallett, and L. E. Brennan, "Rapid Convergence Rate in Adaptive Arrays," *IEEE Trans. Aerosp. Electron. Syst.*, vol. 10-6, pp. 853–863, November 1974.